Plasmonics (2016) 11:851–856
DOI 10.1007/s11468-015-0118-9

Optical Response of Plasmonic Nanohole Arrays: Comparison of Square and Hexagonal Lattices

Yasa Ekşioğlu[1,2] · **Arif E. Cetin**[3] · **Jiří Petráček**[1,4]

Received: 1 May 2015 / Accepted: 7 October 2015 / Published online: 19 October 2015

Abstract Nanohole arrays in metal films allow extraordinary optical transmission (EOT); the phenomenon is highly advantageous for biosensing applications. In this article, we theoretically investigate the performance of refractive index sensors, utilizing square and hexagonal arrays of nanoholes, that can monitor the spectral position of EOT signals. We present near- and far-field characteristics of the aperture arrays and investigate the influence of geometrical device parameters in detail. We numerically compare the refractive index sensitivities of the two lattice geometries and show that the hexagonal array supports larger figure-of-merit values due to its sharper EOT response. Furthermore, the presence of a thin dielectric film that covers the gold surface and mimics a biomolecular layer causes larger spectral shifts within the EOT resonance for the hexagonal array. We also investigate the dependence of the transmission responses on hole radius and demonstrate that hexagonal lattice is highly promising for applications demanding strong light transmission.

✉ Jiří Petráček
petracek@fme.vutbr.cz

[1] Institute of Physical Engineering, Faculty of Mechanical Engineering, Brno University of Technology, Technická 2, 616 69 Brno, Czech Republic

[2] Department of Electrical and Electronics Engineering, Istanbul Kemerburgaz University, Mahmutbey Dilmenler Caddesi No: 26, 34217 Bağcılar Istanbul, Turkey

[3] Department of Biological Engineering and Koch Institute for Integrative Cancer Research, Massachusetts Institute of Technology, Cambridge, MA 02139, USA

[4] CEITEC - Central European Institute of Technology, Brno University of Technology, Technická 10, 616 00 Brno, Czech Republic

Keywords Plasmonics · Extraordinary optical transmission · Nanoholes · Refractive index sensitivity · Grating coupling

Introduction

The ability of light confinement below the diffraction limit with large near-field intensity enhancements through excitation of surface plasmons [1–3] has enabled various applications in biodetection field, i.e., surface-enhanced vibrational spectroscopy [4–10] and label-free biosensing [11–15]. Surface plasmons, propagating at metal surfaces, can be utilized, e.g., in ultra-compact electro-optic modulators [16]. Applications may also rely on different particle-based nanoantennas, which confine electromagnetic radiation to subwavelength dimensions through localized surface plasmon resonances [17–21]. Bringing localized and propagating surface plasmons together in a single platform, i.e., in periodic nanopillar arrays on a conducting layer, optical antenna properties have been significantly improved [22].

An opaque metal film perforated with a subwavelength periodic array of holes can support an extraordinary optical transmission (EOT) [23, 24], i.e., the transmission spectrum of the film exhibits peaks, where the transmission efficiency is orders of magnitude greater than expected by the standard aperture theory [25]. The initial observation by Ebbesen et al. [23] also provided evidence that this phenomenon is related to the excitation of propagating surface plasmons due to periodically patterned metallic surfaces. Since then, numerical and experimental research on metal nanoapertures remarkably increased in a variety of different fields [26–33]. Geometrical parameters (symmetry and periodicity of the aperture array, hole diameter, and film thickness) and material properties play an important role in EOT signal and enable a fine-tuning mechanism of spectral responses [24, 34–36].

Platforms utilizing nanoholes are highly sensitive to surface conditions due to their highly confined local electromagnetic fields, strongly interacting with surrounding medium. For instance, binding of biomolecules triggering a spectral shift within the EOT resonance due to the changes in the local refractive index can be used as an indication of the presence of the analytes on the sensing surface in a label-free manner [37–40]. Recently, utilizing sharp plasmonic Fano resonances, direct detection of single monolayers of antibodies with naked eye has been successfully demonstrated [39].

In this work, we theoretically investigate the effect of geometrical parameters on the performance of refractive index sensors that are based on nanohole arrays and monitor the spectral position of an EOT signal. We consider two aperture systems [39] with nanoholes periodically positioned in two different lattice geometries: square and hexagonal. For both systems, we analyze the spectral quality of the EOT signal and investigate the near-field characteristics of the corresponding plasmonic modes that play the dominant role for EOT. We model the refractive index sensing capabilities of two systems by introducing different refractive indices of bulk solutions as well as a dielectric slab covering the metal interface. Finally, we investigate the dependence of the EOT signal on hole radius.

Methods

We consider square and hexagonal nanohole arrays that are formed trough a gold film and a silicon nitride layer [39] as schematically illustrated in Fig. 1. According to the classical diffraction theory of apertures by Bethe, the transmittance normalized to the aperture area scales with aperture radius r and wavelength λ as $(r/\lambda)^4$, which implies a strong reduction in subwavelength regime [25]. However, nanohole arrays support strong transmission peaks that are related to excitation of propagating surface plasmons corresponding to the different grating orders. These EOT signals, labeled by integers (m, n) that define the grating orders, are approximately located at wavelengths that obey the grating coupling condition [23, 39]:

$$\vec{k}_{SP} = \vec{k}_{inc,||} + m\vec{b}_1 + n\vec{b}_2 \quad (1)$$

Here, $\vec{k}_{SP}$ is the surface plasmon wavevector, $\vec{k}_{inc,||}$ is the component of the wavevector of the incident photons in the plane of the metal surface, $\vec{b}_1$ and $\vec{b}_2$ are the elementary reciprocal lattice vectors, for square lattice $\left|\vec{b}_1\right| = \left|\vec{b}_2\right| = \frac{2\pi}{P}$ and for hexagonal lattice $\left|\vec{b}_1\right| = \left|\vec{b}_2\right| = \frac{4\pi}{\sqrt{3}P}$, and P is the period of the array (the lattice constant). Dispersion relation for surface plasmon is shown in Eq. (2):

$$k_{SP} = k_0\sqrt{\frac{\varepsilon_d\varepsilon_m}{\varepsilon_d + \varepsilon_m}} \quad (2)$$

where ε_m and ε_d are the dielectric constants of the metal and dielectric layers, respectively, and k_0 is the wavenumber in vacuum. Utilizing Eqs. (1) and (2), one can estimate the spectral positions of the EOT signals at normal incidence supported by the nanohole arrays within the square, Eq. (3), and hexagonal, Eq. (4), lattice format:

$$\lambda_{res} = \frac{P}{\sqrt{m^2 + n^2}}\sqrt{\frac{\varepsilon_d\varepsilon_m}{\varepsilon_d + \varepsilon_m}} \quad (3)$$

$$\lambda_{res} = \frac{P}{\sqrt{\frac{4}{3}\left(m^2 + mn + n^2\right)}}\sqrt{\frac{\varepsilon_d\varepsilon_m}{\varepsilon_d + \varepsilon_m}} \quad (4)$$

In our analysis, we focus on Au/Air(1,0) mode (m=1, n=0, ε_d=1). The dielectric constant of gold ε_m is taken from ref. [41], and the refractive index of silicon nitride (required for rigorous simulations) is set to 2.16, which is the average refractive index within the visible spectrum. We assume a normally incident plane wave, linearly polarized along the x-direction and propagating along the z-direction (as schematically illustrated in Fig. 1a). For rigorous simulations, we employ the finite-difference time-domain (FDTD) technique [42], where we use 2-nm mesh size in all directions.

Results

Figure 2a shows the transmission response of the two nanohole arrays. Square and hexagonal lattices have different

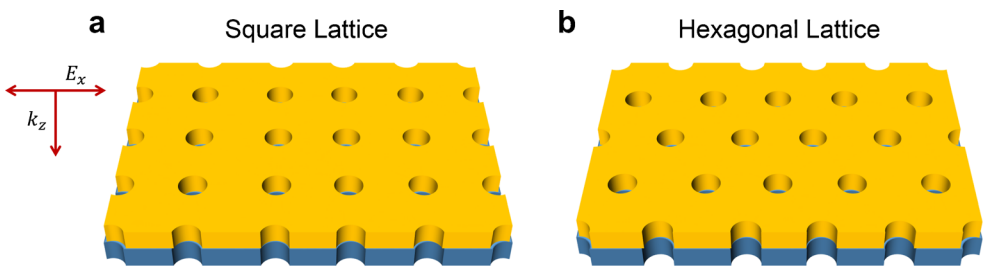

Fig. 1 Schematic view of nanohole arrays with **a** square and **b** hexagonal lattices; *yellow* and *blue* colors mark gold and silicon nitride layers, respectively. Polarization and propagation directions of incident light are also shown in (**a**)

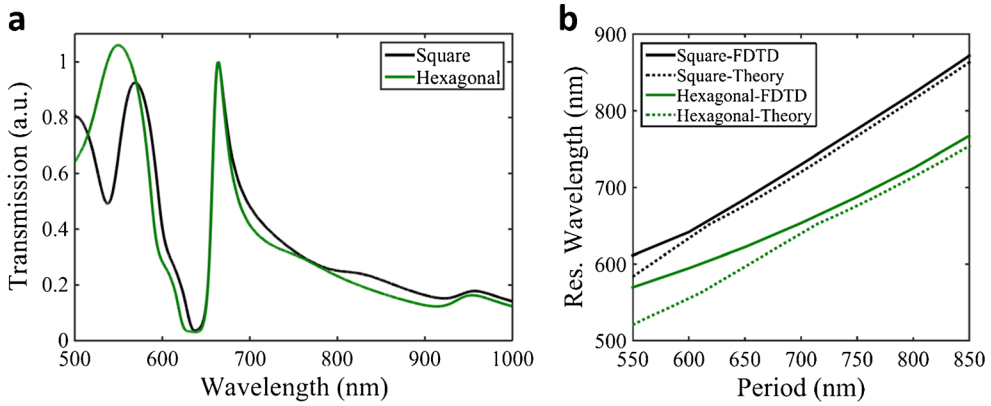

Fig. 2 **a** EOT spectra of the nanoholes for square lattice with period P= 600 nm (*black*) and hexagonal lattice with period P=684 nm (*green*). **b** Resonance wavelength vs. period calculated for Au/Air(1,0) mode; *solid lines* indicate the FDTD calculation (square lattice = *black*, hexagonal lattice = *green*) while *dashed lines* indicate the theoretical model (square lattice = *black*, hexagonal lattice = *green*). Other geometrical parameters for both (**a**) and (**b**): hole radius r =100 nm and thicknesses of gold and silicon nitride layers are 120 and 70 nm, respectively

periods in order to have Au/Air(1,0) modes at the similar spectral positions. Here, the nanoholes with hexagonal lattice show sharper linewidth compared to those with square lattice, i.e., 15.1 vs. 16.6 nm. Figure 2b shows the resonance wavelength with respect to array periodicity, where the solid lines (black=square lattice and green=hexagonal lattice) represent the FDTD results while the dashed curves were calculated from Eqs. (3) and (4), respectively. The discrepancy between theoretical estimations and rigorous simulations is mainly due to the presence of air holes in the metal film. The theoretical model only accounts for the propagating surface plasmons, while the plasmonic nanoholes can also excite localized surface plasmons whose properties depend on the aperture geometry. Thus, the EOT phenomenon uniquely combines propagating and localized surface plasmons as will be shown in the following section. As a result, an increase in the hole radius shifts the EOT resonance to longer wavelengths (see also Fig. 6). Similarly, the increase in metal thickness shifts the

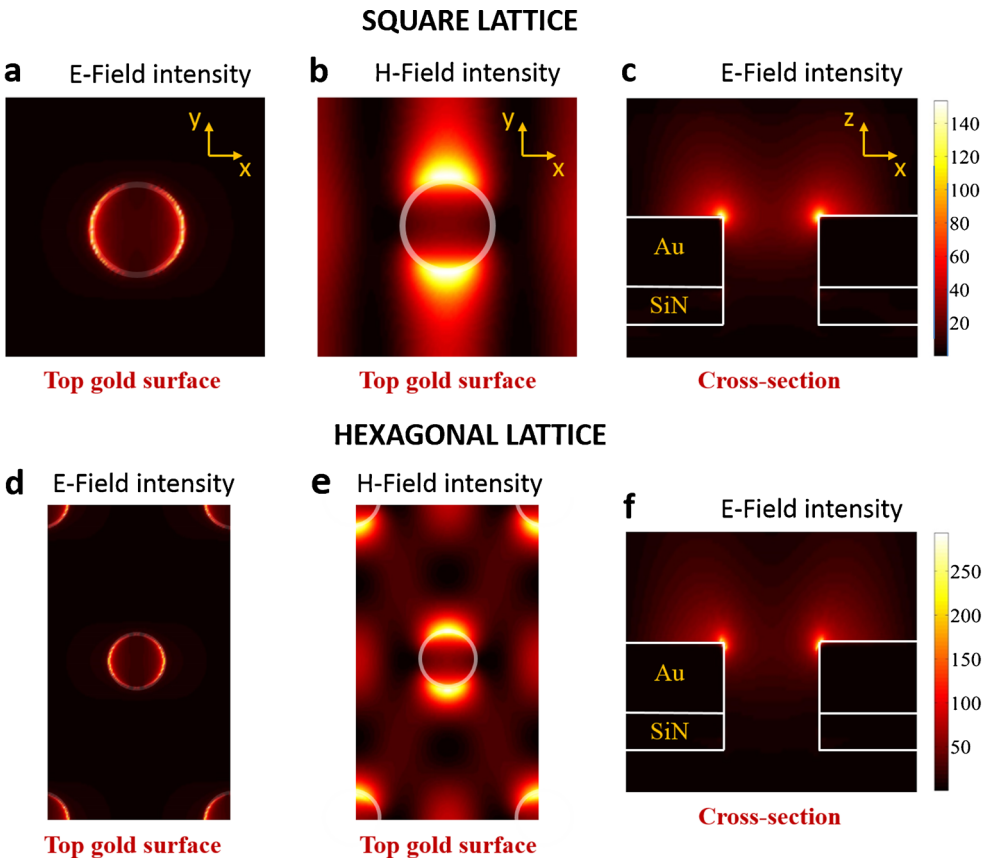

Fig. 3 Electric and magnetic field intensity distributions calculated at the Au/Air(1,0) resonance for two nanohole systems. Electric field intensity distributions at the top metal surface for **a** square and **d** hexagonal lattices. Magnetic field intensity distributions at the top metal surface for **b** square and **e** hexagonal lattices. Cross-sectional electric field intensity distributions for **c** square and **f** hexagonal lattices. The structural parameters are as in Fig. 2a

resonance to longer wavelengths (not shown here), which has a negligible effect here as the assumed metal film is relatively thick.

Figure 3 shows the near-field distributions at the resonance. Electric field intensity distributions, calculated at the top surface of the metal film (Fig. 3a, d), indicate the excitation of localized surface plasmons which have dipolar character, allowing large near-field enhancements as well as strong EOT signals in the far field. Here, strong near fields are localized at the rims of the aperture along the polarization direction (x). Magnetic field intensity distributions calculated at the top surface of the metal film (Fig. 3b, e) show that the plasmonic hot spots around the rims of the nanoholes along y-direction are due to the excitations of localized surface plasmons. For square lattice, the standing field pattern along x-direction is due to the simultaneous excitation of two counter-propagating surface plasmons that correspond to Au/Air(±1,0) modes (Fig. 3b) [12]. For hexagonal lattice, the standing field pattern has more complex form as it appears along two directions that make angles of +30° and −30° with x-axis and correspond to the excitation of Au/Air(±1,0) and Au/Air(±1,∓1) modes, respectively (Fig. 3e). As shown in the cross-sectional field profile (xz-direction) in Fig. 3c, f, large electromagnetic fields are localized at the aperture tips (top gold surface) and extend extensively within the medium in the vicinity of the aperture arrays. These large and highly accessible local electromagnetic fields strongly improve the sensitivity of the aperture systems to the change in the local refractive index, which will be analyzed in the following section.

As nanohole arrays support large and accessible near fields, the spectral location of their strong transmission resonances highly depends on the change in the refractive index of the adjacent medium n. We then quantify this dependence through wavelength sensitivity, which is defined as the ratio between the resonance wavelength shift and the change in refractive index ($S=\Delta\lambda/\Delta n$) [39]. Figure 4 presents the calculated resonance wavelength of Au/Medium(1,0) mode for various media including DI water (n=1.33), acetone (n=1.35), ethanol (n=1.36), and IPA (n=1.37). Here, nanohole arrays with square lattice (black line) show a wavelength sensitivity of 640 nm/refractive index unit (RIU), whereas the one with hexagonal lattice (green line) support a smaller sensitivity of 610 nm/RIU. On the other hand, supporting sharper resonances with full-width half maximum (FWHM) of 15.1 vs. 16.6 nm, hexagonal lattice exhibits larger figure-of-merit values (FOM=S/FWHM) compared to square one as 40.4 vs. 38.5.

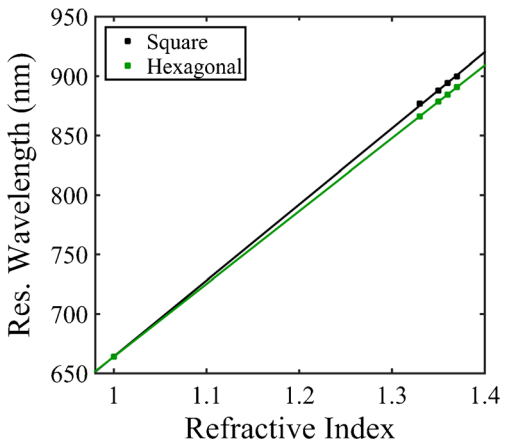

Fig. 4 Resonance wavelength of Au/Medium(1,0) mode vs. refractive index of the adjacent medium (air, DI water, acetone, ethanol, IPA) for square (*black line*) and hexagonal (*green line*) lattices. The other structural parameters are as in Fig. 2a

In order to better quantify the sensing capabilities of the nanohole systems, we numerically analyzed the apertures, in which the gold surface was covered with a 10-nm dielectric film with a refractive index of n=1.6, which accounts for a biomolecular layer sticking on the surface. As shown in Fig. 5a, b, hexagonal lattice shows larger sensitivity compared to square one, i.e., Au/Air(1,0) modes shift to longer wavelengths by $\Delta\lambda$=24.8 nm vs. $\Delta\lambda$=23.8 nm. Furthermore, as

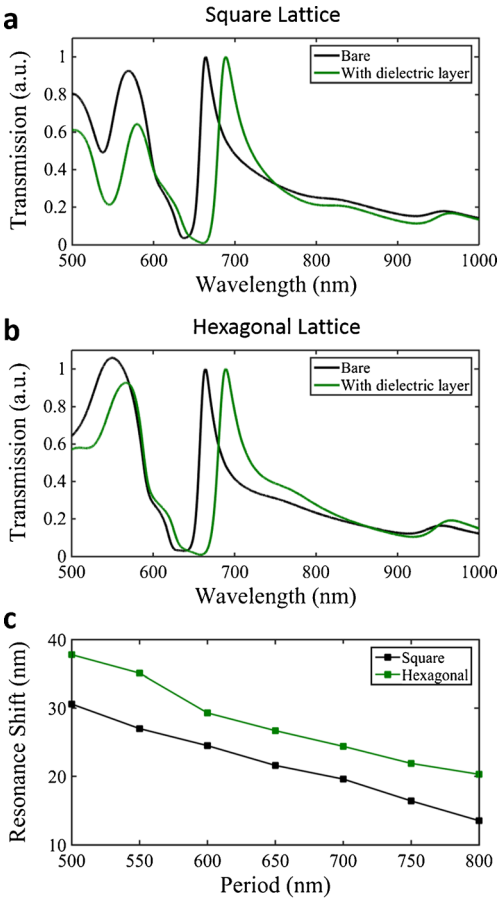

Fig. 5 Variations of EOT spectra for **a** square and **b** hexagonal lattice; *Bare* indicates results of Fig. 2a, and *With dielectric layer* indicates the gold surface covered with a 10-nm dielectric film with the refractive index n=1.6. **c** Spectral shift of Au/Air(1,0) mode caused by the dielectric film vs. the period for both the lattices

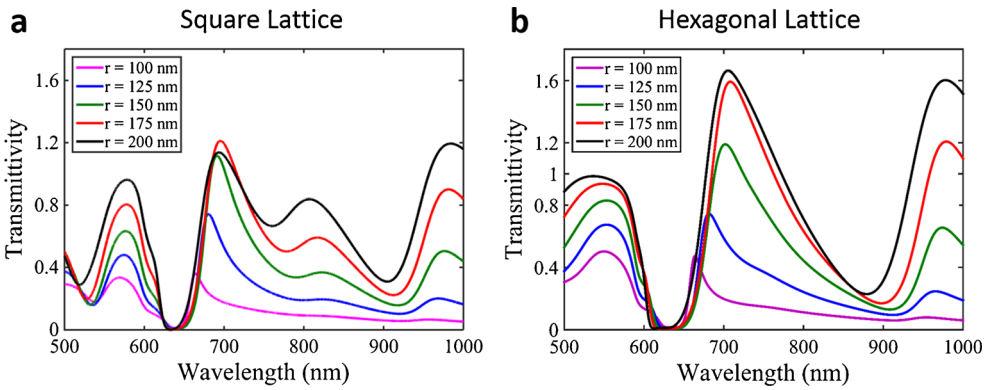

Fig. 6 EOT spectra of nanohole arrays for **a** square and **b** hexagonal lattices and different values of the hole radius *r*. The other structural parameters are as in Fig. 2a

presented in Fig. 5c, increasing periodicity decreases the spectral shifts in both arrays. Figure 5c also shows that for the same periodicity, hexagonal lattice supports much larger spectral shifts compared to square one; the increase in the shift is about 7 nm, which is highly important for biosensing applications.

Finally, we investigate the effect of radius on the transmission spectra in Fig. 6a, b for square and hexagonal lattices, respectively. As inferred from the conventional diffraction theory, transmission of light from apertures increases for larger hole diameters. In order to eliminate this additional effect, we compare the transmittivity (the transmission normalized to the area occupied by the holes) of each structure for different hole diameters. For both aperture systems, we observe a similar behavior such that transmittivity increases for larger aperture radiuses. Here for the same radius, hexagonal lattice supports larger transmittivity. More importantly, for the nanoholes with hexagonal lattice, Au/Air(1,0) mode is well defined even for larger radiuses while improving the transmission capability. This characteristic is highly important for imaging-based biosensing studies demanding strong light transmission without suffering from undesired variations within spectral line shape. In contrast, the system with square lattice strongly suffers from the spectral shoulder that appears on the right side of Au/Air(1,0) mode, which makes monitoring this spectral feature complicated. As an additional note, we observe that changes in the thicknesses of metal and dielectric layers result in identical variations within transmission spectra (not shown here) for both systems as they have identical effects on physical phenomena playing the role for EOT.

Conclusion

In this article, we theoretically investigated EOT responses of nanohole arrays with square and hexagonal lattice symmetries that are applicable in refractive index sensing. For similar resonance wavelengths, both arrays yield similar wavelength sensitivities; however, hexagonal array supports larger figure-of-merit values due to its spectrally sharp EOT signal compared to square one. In order to demonstrate the sensing capabilities of both lattice configurations, we modeled biomolecules sticking on the gold surface by a 10-nm dielectric layer. In this case, spectral resonance shift caused by the dielectric film is larger for hexagonal lattice; the difference increases when the lattices have the same period. Finally, we found that the resonance in hexagonal lattice is well defined even for larger hole radiuses; the observation demonstrates that this lattice is highly advantageous over the square one for applications demanding strong light transmission.

Acknowledgments This research is supported by the project CZ.1.07/2.3.00/30.0039 of Brno University of Technology. J. Petráček acknowledges the support of CEITEC - Central European Institute of Technology (project CZ.1.05/1.1.00/02.0068), in the framework of European Regional Development Fund.

References

1. Stern EA, Ferrell RA (1960) Surface plasma oscillations of a degenerate electron gas. Phys Rev 120:130–136
2. Ozbay E (2006) Plasmonics: merging photonics and electronics at nanoscale dimensions. Science 311:189–193
3. Maier SA (2007) Plasmonics: fundamentals and applications. Springer, New York
4. Osawa M, Ikeda M (1991) Surface-enhanced infrared absorption of p-nitrobenzoic acid deposited on silver island films: contributions of electromagnetic and chemical mechanisms. J Phys Chem 95: 9914–9919
5. Kneipp K, Wang Y, Kneipp H, Perelman LT, Itzkan I, Dasari RR, Field MS (1997) Single molecule detection using surface-enhanced Raman scattering (SERS). Phys Rev Lett 78:1667–1670
6. Kundu J, Le F, Nordlander P, Halas NJ (2008) Surface enhanced infrared absorption (SEIRA) spectroscopy on nanoshell aggregate substrates. Chem Phys Lett 452:115–119
7. Adato R, Yanik AA, Amsden JJ, Kaplan DL, Omenetto FG, Hong MK, Erramili S, Altug H (2009) Ultra-sensitive vibrational spectroscopy of protein monolayers with plasmonic nanoantenna arrays. Proc Natl Acad Sci U S A 106:19227–19232
8. Aksu S, Cetin AE, Adato R, Altug H (2013) Plasmonically enhanced vibrational biospectroscopy using low-cost infrared antenna arrays by nanostencil lithography. Adv Opt Mater 1:798–803

9. Cetin AE, Etezadi D, Altug H (2014) Accessible nearfields by nanoantennas on nanopedestals for ultrasensitive vibrational spectroscopy. Adv Opt Mater 2:866–872
10. Cetin AE, Turkmen M, Aksu S, Etezadi D, Altug H (2015) Multi-resonant compact nanoaperture with accessible large nearfields. Appl Phys B 118:29–38
11. Kabashin AV, Evans P, Pastkovsky S, Hendren W, Wurtz GA, Atkinson R, Pollard R, Podolskiy VA, Zayats AV (2009) Plasmonic nanorod metamaterials for biosensing. Nat Mater 8: 867–871
12. Artar A, Yanik AA, Altug H (2009) Fabry–Pérot nanocavities in multilayered plasmonic crystals for enhanced biosensing. Appl Phys Lett 95:051105
13. Cetin AE, Altug H (2012) Fano resonant ring/disk plasmonic nanocavities on conducting substrates for advanced biosensing. ACS Nano 6:9989–9995
14. Im H, Bantz KC, Lee SH, Johnson TW, Haynes CL, Oh SH (2013) Self-assembled plasmonic nanoring cavity arrays for SERS and LSPR biosensing. Adv Mater 25:2678–2685
15. Cetin AE, Mertiri A, Huang M, Erramilli S, Altug H (2013) Thermal tuning of surface plasmon polaritons using liquid crystals. Adv Opt Mater 1:915–920
16. Cetin AE, Yanik AA, Mertiri A, Erramilli S, Mustecaplioglu OE, Altug H (2012) Field-effect active plasmonics for ultracompact electro-optic switching. Appl Phys Lett 101:121113
17. Novotny L (2007) Effective wavelength scaling for optical antennas. Phys Rev Lett 98:266802
18. Cubukcu E, Capasso F (2009) Optical nanorod antennas as dispersive one-dimensional Fabry-Pérot resonators for surface plasmons. Appl Phys Lett 95:201101
19. Cetin AE, Turkmen M, Aksu S, Altug H (2012) Nanoparticle-based metamaterials as multiband plasmonic resonator antennas. IEEE Trans Nanotechnol 11:208–212
20. Cetin AE, Artar A, Turkmen M, Yanik AA, Altug H (2011) Plasmon induced transparency in cascaded π-shaped metamaterials. Opt Express 19:22607–22618
21. Cetin AE (2015) FDTD analysis of optical forces on bowtie antennas for high-precision trapping of nanostructures. Int Nano Lett 5: 21–27
22. Cetin AE, Yanik AA, Yilmaz C, Somu S, Busnaina A, Altug H (2011) Monopole antenna arrays for optical trapping, spectroscopy, and sensing. Appl Phys Lett 98:111110
23. Ebbesen TW, Lezec HJ, Ghaemi HF, Thio T, Wolff PA (1998) Extraordinary optical transmission through sub-wavelength hole arrays. Nature 391:667–669
24. Genet C, Ebbesen TW (2007) Light in tiny holes. Nature 445:39–46
25. Bethe HA (1944) Theory of diffraction by small holes. Phys Rev 66:163–182
26. Gordon R, Brolo AG, McKinnon A, Rajora A, Leathem B, Kavanagh KL (2004) Strong polarization in the optical transmission through elliptical nanohole arrays. Phys Rev Lett 92:037401
27. Najiminaini M, Vasefi F, Kaminska B, Carson JJL (2010) Experimental and numerical analysis on the optical resonance transmission properties of nano-hole arrays. Opt Express 18: 22255–22270
28. Turkmen M, Aksu S, Cetin AE, Yanik AA, Altug H (2011) Multi-resonant metamaterials based on UT-shaped nano-aperture antennas. Opt Express 19:7921–7928
29. Yanik AA, Huang M, Artar A, Chang TY, Altug H (2010) Integrated nanoplasmonic-nanofluidic biosensors with targeted delivery of analytes. Appl Phys Lett 96:021101
30. Huang M, Galarreta BC, Cetin AE, Altug H (2013) Actively transporting virus like analytes with optofluidics for rapid and ultrasensitive biodetection. Lab Chip 13:4841–4847
31. Coskun AF, Cetin AE, Galarreta BC, Alvarez DA, Altug H, Ozcan A (2014) Lensfree optofluidic plasmonic sensor for real-time and label-free monitoring of molecular binding events over a wide field-of-view. Sci Rep 4:1–7
32. Yuan J, Xie Y, Geng Z, Wang C, Chen H, Kan Q, Chen H (2015) Enhanced sensitivity of gold elliptic nanohole array biosensor with the surface plasmon polaritons coupling. Opt Mater Express 5:818–826
33. Degiron A, Lezec HJ, Barnes WL, Ebbesen TW (2002) Effects of hole depth on enhanced light transmission through subwavelength hole arrays. Appl Phys Lett 81:4327–4329
34. van der Molen KL, Koerkamp KJK, Enoch S, Segerink FB, van Hulst NF, Kuipers L (2005) Role of shape and localized resonances in extraordinary transmission through periodic arrays of subwavelength holes: experiment and theory. Phys Rev B 72:045421
35. Sun M, Tian J, Han S, Li Z, Cheng B, Zhang D, Jin A, Yang H (2006) Effect of the subwavelength hole symmetry on the enhanced optical transmission through metallic films. J Appl Phys 100: 024320
36. Rodrigo SG, García Vidal FJ, Martín-Moreno L (2008) Influence of material properties on extraordinary optical transmission through hole arrays. Phys Rev B 77:075401
37. Yanik AA, Huang M, Kamohara O, Artar A, Geisbert TW, Connor JH, Altug H (2010) An optofluidic nanoplasmonic biosensor for direct detection of live viruses from biological media. Nano Lett 10:4962–4969
38. Cetin AE, Coskun AF, Galarreta BC, Huang M, Herman D, Ozcan A, Altug H (2014) Handheld high-throughput plasmonic biosensor using computational on-chip imaging. Light Sci Appl 3:1–10
39. Yanik AA, Cetin AE, Huang M, Artar A, Mousavi SH, Khanikaev A, Connor JH, Shvets G, Altug H (2011) Seeing protein monolayers with naked eye through plasmonic Fano resonances. Proc Natl Acad Sci U S A 108:11784–11789
40. Cetin AE, Etezadi D, Galarreta BC, Busson MP, Eksioglu Y, Altug H (2015) Plasmonic nanohole arrays on a robust hybrid substrate for highly sensitive label-free biosensing. ACS Photon 2:1167–1174
41. Palik ED (ed) (1985) Handbook of optical constants of solids. Academic, Orlando
42. Lumerical FDTD solutions software: www.lumerical.com